ELSEVIER

Journal of Power Sources 101 (2001) 60–71

JOURNAL OF POWER SOURCES

www.elsevier.com/locate/jpowsour

Numerical analysis of output characteristics of tubular SOFC with internal reformer

Susumu Nagata*, Akihiko Momma, Tohru Kato, Yasuhiro Kasuga

Electrotechnical Laboratory, 1-1-4 Umezono, Tsukuba, Ibaraki 305-8568, Japan

Received 5 June 2000; received in revised form 6 November 2000; accepted 17 January 2001

Abstract

In the solid oxide fuel cell (SOFC) system, the internal reforming of raw fuel will act as an efficient cooling system. To realize this cooling system, a special design of the internal reformer is required to avoid the inhomogeneous temperature distribution caused by the strong endothermic reforming reaction at the entrance of the internal reformer. For this purpose, a tubular internal reformer with adjusted catalyst density can be inserted into the tubular SOFC stack. By arranging this, the raw fuel flows along the axis of the internal reformer to be moderately reformed and returns at the end of the internal reformer as a sufficiently reformed fuel.

In this paper, the output characteristics of this configuration are simulated using mathematical models, in which one-dimensional temperature and molar distributions are computed along the flow direction. By properly mounting the catalyst density in the internal reformer, the temperature distribution of the cell stack becomes moderate, and the power generation efficiency and the exhaust gas temperature are higher. Effects of other operating conditions such as fuel recirculation, fuel inlet temperature, air recirculation and air inlet temperature are also examined under the condition where the maximum temperature of the stack is kept at 1300 K by adjusting the air flow rate. Under this condition, these operating conditions exert a considerable effect on the exhaust temperature but have a slight effect on the efficiency.

Keywords: Solid oxide fuel cell (SOFC); Tubular SOFC; Internal reform; Simulation

1. Introduction

Tubular solid oxide fuel cells (SOFCs) have been pointed out to have advantages with respect to mechanical stresses developed by seals and thermal stresses caused by the temperature distribution along the cell axis, in comparison with planar SOFCs [1]. However, leveling of the temperature distribution is still required to avoid cell deterioration due to the higher local temperature. The higher temperature may lead to electrode sintering and chemical reaction between the electrode and the electrolyte. Therefore, the temperature distribution has to be restricted in a narrow range.

The reforming of raw fuel is an endothermic reaction. Therefore, the internal reforming can be used to cool the cell stack, only if some design is contrived to avoid the inhomogeneous temperature distribution caused by the strong reforming reaction at the inlet of the internal reformer. To fill this requirement, the internal reformer should be separated from the fuel electrode to adjust the catalyst density. For this purpose, a tubular internal reformer with a thin or graded catalyst density can be inserted into the tubular cell. The raw fuel will flow then along the axis of the reformer to be reformed moderately and will change its flow direction as a sufficiently reformed fuel at the end of the internal reformer.

There is also another advantage of the internal reforming avoiding the heat loss that cannot be avoided in the external reforming.

In this paper, the schematic structure of the tubular SOFC equipped with an internal reformer is presented, and the effects of the internal reforming and other operating conditions are discussed by numerical simulations.

2. SOFC system equipped with internal reformer

A schematic structure of the SOFC system having both a pre-reformer and an internal reformer is shown in Fig. 1. In this figure, one cell stack with an internal reformer and two air supply tubes are shown. In a real system, many stacks, internal reformers and air tubes have to be arranged. The enlarged drawing of the stack will be shown later in Fig. 3.

* Corresponding author. Fax: +81-298-61-5791.
E-mail address: e6627@etl.go.jp (S. Nagata).

0378-7753/01/$ – see front matter
PII: S0378-7753(01)00547-X

Nomenclature

A_c	activity of carbon
A_g	cross-section of gas CV concerned (cm^2)
A_{ref}	reforming area per length (cm^2/cm)
A_s	cross-sectional area of solid CV concerned (cm^2)
$A_s k_s$	equivalent value considering the effect of multilayers
c	total molar concentration (mol/cm^3)
C_{p_j}	heat capacity of gas species j (J/mol)
d_e	equivalent diameter (cm)
D_{ij}	diffusivity between gas species i and j in porous media (cm^2/s)
D^0_{ij}	diffusivity between gas species i and j in free flow (cm^2/s)
E	electromotive force of relevant position of cell at T (V)
$E(i)$	electromotive force of CV(i) concerned
$E_0(T)$	standard electromotive force at T (V)
F	Faraday's constant (96485 C/mol)
ΔG_{act}	activation energy (J/mol)
h_g	heat transfer coefficient of mixed gas (W/cm^2 K)
$H_j(T)$	enthalpy of gas species j at T (J/mol)
$H^0_j(T)$	heat of formation of gas species j at T (J/mol)
$\Delta H^0_{CH_4}$	enthalpy change in combustion of CH_4 at 298 K in HHV (J/mol)
ΔH^0_{1300}	enthalpy change of reaction at 1300 K (kJ/mol)
$I_a(i)$	current flowing in air electrode of CV(i) (A)
$I_e(i)$	current flowing in electrolyte of CV(i) (A)
$I_f(i)$	current flowing in fuel electrode of CV(i) (A)
I_0	load current (A)
J	current density in electrolyte (A/cm^2)
J_0	exchange current density (A/cm^2)
k_g	thermal conductivity of gas (W/cm K)
k_s	thermal conductivity of solid (W/cm K)
K_c	equilibrium constant of the Bourdouard reaction
K_{ox}	equilibrium constant of oxidation of hydrogen
K_s	equilibrium constant of water gas shift reaction
M_j	mole flow rate of gas species j (mol)
M'_j	mole flow rate of air gas species j (mol)
δM_{CH_4}	mole of reformed methane in CV concerned (mol/s)
δM_{CO_2}	mole of CO_2 generated by water gas shift reaction in CV concerned (mol/s)
N_{cell}	number of cells in stack
N_j	mole flux of gas species j (mol/cm^2 s)
P_j	partial pressure of gas species j (atm)
$P_{i,B}$	partial pressure of gas species j at boundary between electrolyte and fuel electrode (atm)
$P_{O_2,B}$	partial pressure of oxygen at boundary between electrolyte and fuel electrode (atm)
P'_{O_2}	partial pressure of oxygen in air (atm)
$P'_{O_2,B}$	partial pressure of oxygen at boundary between electrolyte and air electrode (atm)
$Q_{cell,f}$	heat migration to side wall with fuel flow due to cell reaction (W)
$Q_{cell,ox}$	heat migration to side wall with oxygen flow due to cell reaction (W)
$Q_{conv}(i)$	enthalpy migration due to gas flow to CV(i) (W)
Q_{heat}	heat generated in CV concerned (W)
Q_{joul}	heat generated by Joule heating (W)
Q_{rad}	net heat input by radiation (W)
Q_{react}	enthalpy migration to side wall due to convection (W)
Q_{reform}	heat generated by reforming of methane (W)
Q_{shift}	heat generated by water gas shift reaction (W)
Q^g_{cond}	heat input due to heat conduction from neighboring gas CVs (W)
$\sum_j Q_j$	summation of quantity Q in relevant gas flow
$\sum_j^{exhaust} Q_j$	summation of quantity Q_j in exhaust gas
$\sum_j^{input\ air} Q_j$	summation of quantity Q_j in input air
r	radial distance in cylindrical coordinate (cm)
r_{sub}	radius of substrate (cm)
R	universal gas constant (8.31441 J/(mol K))
R_a	branch resistance of air electrode (Ω)
R_{CH_4}	rate of reforming of methane (mol/(g Ni s))
R_e	branch resistance of electrolyte (Ω)
R_{ecf}	recirculation rate of fuel
R_f	branch resistance of fuel electrode (Ω)
R_{int}	branch resistance of interconnecting material (Ω)
R_r	reforming rate of methane
S_s	side wall area of CV concerned (cm^2)
S_{s1}	side wall area of inside CV (cm^2)
S_{s2}	side wall area of outside CV (cm^2)
T, T_0	temperature (K)
T_a	temperature of air (K)
T_{a0}	air inlet temperature to system (K)
T_{ain}	air inlet temperature to cell (K)
$T_{cell}(i)$	temperature of cell CV(i) (K)
$T_{cell,max}$	maximum temperature of cell stack (K)
$T_f(i)$	temperature of fuel CV(i) (K)
T_{fin}	fuel inlet temperature to cell (K)
T_{f0}	fuel inlet temperature to system (K)
$T_g(i)$	temperature of gas CV(i) (K)
T_{max}	maximum allowable temperature (K)
$T_{ox}(i)$	temperature of oxidant CV(i) (K)
T_{out}	exhaust gas temperature from SOFC system (K)
$T_s(i)$	temperature of solid CV(i) (K)

T_{sx}	temperature of opposite solid CV (K)
U_f	fuel utilization rate
U_{ox}	oxygen utilization
V_{act}	activation polarization (V)
$V_{act,f}$	activation polarization of fuel electrode (V)
$V_{act,ox}$	activation polarization of air electrode (V)
V_{cell}	average value of cell voltage (V)
V_{cons}	concentration polarization
V_p	polarization voltage (V)
$V_p(i)$	polarization voltage of CV(i) (V)
V_t	load voltage of cell stack (V)
x	flow direction coordinate (cm)
δx	length of CV concerned (cm)
X_j	mole fraction of gas species j
$X_{J,B}$	mole fraction of gas species j at boundary between electrolyte and fuel electrode
X'_{O_2}	mole fraction of oxygen in oxidant
$X'_{O_2,B}$	mole fraction of oxygen at boundary between electrolyte and air electrode
W_{cat}	catalyst Ni weight density (g/cm^2)

Greek letters

α	transfer coefficient
β	proportional constant (1/cm^2 Ω)
ε	porosity
γ	reaction order of oxygen
η_{dc}	thermal efficiency of SOFC in HHV
σ_0	interface conductivity (1/cm^2 Ω)

Subscripts and superscripts

B	boundary between electrode and electrolyte
f	fuel
g	gas (fuel, fuel (reformed fuel), air, oxidant)
ox	oxidant
s	solid (tube, cell, internal reformer)

The raw fuel, methane, comes into the pre-reformer at the left end, then goes into the internal reformer. The reformed fuel changes its direction and flows back through the annulus formed by the internal reformer and the cell stack. The air comes into the air supply tube at the right end after being preheated by the exhaust gas through the heat exchanger. The air also changes its direction at the left end and flows back as an oxidant. Some parts of the spent gases are recirculated using ejectors to preheat the inlet gases.

The recirculated spent fuel also supplies the steam required to reform methane.

The cell stack is a power generator; on the other hand it is a heater. In the SOFC system, the cooling of the cell is carried out by the reactants at the lower temperature and the reforming reaction. The flow rates of the reactants, the gas recirculation rates, the inlet temperatures of the reactants and the rate of reforming are interdependent under the restricting condition to maintain the maximum temperature of the cell stack at the preset value.

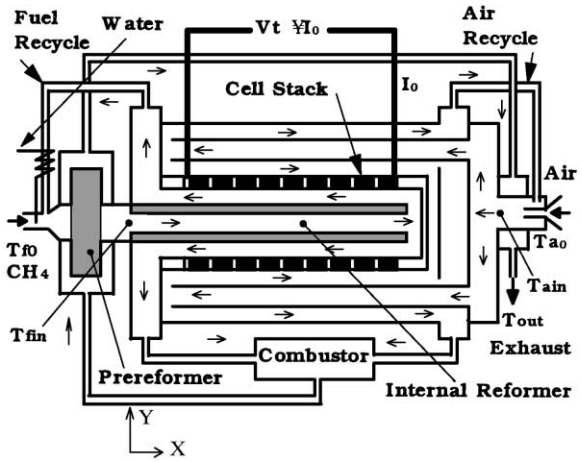

Fig. 1. Schematic of SOFC system with pre-reformer and internal reformer.

The residual spent gases are burned in a combustor to obtain the higher temperature of the exhaust gas out of the SOFC system. The combustion gas heats the pre-reformer and the supplied air sequentially.

If the catalyst, Ni, is loaded densely and uniformly on the internal surface of the internal reformer in the manner used for the fuel electrode, the reforming reaction may be completed at the entrance, and this region may be cooled strongly to distort the whole temperature distribution. To avoid this, the density of the catalyst has to be thin in order to complete the reforming reaction at the end of the internal reformer. If a more complicated design can be allowed, the density has to be thinner at the inlet region and thicker at the outlet region. By this grading of the catalyst density, the temperature distribution may become flatter.

3. Definition of thermal efficiency of SOFC system

The thermal efficiency of the methane-fuelled SOFC (abbreviated ''efficiency'' here), η_{dc} is defined as

$$\eta_{dc} = \frac{V_t I_0}{M_{CH_4}(-\Delta H^0_{CH_4})} = \frac{V_{cell}}{1.1534} U_f, \tag{1}$$

because

$$M_{CH_4} = \frac{I_0 N_{cell}}{8 F U_f}, \qquad V_{cell} = \frac{V_t}{N_{cell}}, \tag{2}$$

where V_t is the dc output voltage of cell stack, I_0 the load current, M_{CH_4} the mass flow of input methane, $\Delta H^0_{CH_4}$ the enthalpy change in the combustion of methane at 298 K, V_{cell} the average cell voltage, U_f the fuel utilization rate and N_{cell} the number of cells in the stack.

As can be seen in Eq. (1), U_f must be higher to obtain higher efficiency; however, if U_f is too high, the fuel will be depleted at the end of the cell and the cell voltage will drop

substantially. Therefore, U_f is chose to be 85% in our system referring to the reported experimental results [2–4].

4. Numerical models for simulation

For the simulation of the SOFC system with the internal reformer, we need numerical models of reforming the cell and heat migration. These models will be described sequentially.

In gas flow modeling, plug flow is assumed in the main flow region, and flow is assumed in the porous media such as the electrodes and the substrate.

A set of the cell stack equipped with an internal reformer and an air injection tube will be considered from now on, assuming periodicity in the *Y*-axis direction. Namely, the effect of the heat loss from the vessel is ignored. The *X*-axis originates from the inlet of the internal reformer as indicated in Fig. 1.

4.1. Reforming

In the reforming of methane with steam, the dominant reactions are the following two reactions:

$$CH_4 + H_2O = 3H_2 + CO, \quad \Delta H^0_{1300} = 227.5\,\mathrm{kJ/mol} \tag{3}$$

$$CO + H_2O = H_2 + CO_2, \quad \Delta H^0_{1300} = -31.8\,\mathrm{kJ/mol} \tag{4}$$

The reaction given by Eq. (3) is a slow and highly endothermic reaction, and the reaction given by Eq. (4) is a fast and weak exothermic reaction [5]. The latter reaction, the water gas shift reaction, is assumed to be in equilibrium at the reforming temperature.

4.1.1. Pre-reforming of methane

In pre-reforming, carbon formation may take place under unfavorable conditions. The dominant reactions for the carbon formation are the following reactions [6,7]:

$$2CO = CO_2 + C \qquad (\text{Boudouard}), \tag{5}$$

$$CO + H_2 = H_2O + C \qquad (\text{CO hydrogenation}), \tag{6}$$

$$CH_4 = 2H_2 + C \qquad (\text{CH}_4 \text{ decomposition}). \tag{7}$$

The activity of carbon, A_c, of Eq. (5) is given as

$$A_c = \frac{K_c P^2_{CO}}{P_{CO_2}}. \tag{8}$$

The activities of carbon in Eqs. (6) and (7) can be given in the same manner. These activities are equal in equilibrium. In nonequilibrium, the lowest activity has the priority to be checked. Activity exceeding 1.0 indicates the initiation of carbon formation. As mentioned above, water vapor necessary for the reforming and the suppression of carbon formation is supplied by the recirculation of the spent fuel. The changes in the carbon activity, A_c, and the methane reforming rate, R_r (equal to the ratio reformed CH_4/input CH_4), with the reforming temperature and the fuel recirculation rate, R_{ecf}, are shown in Fig. 2. Both the reforming rate and the carbon activity are sensitive to the temperature and the fuel recirculation rate.

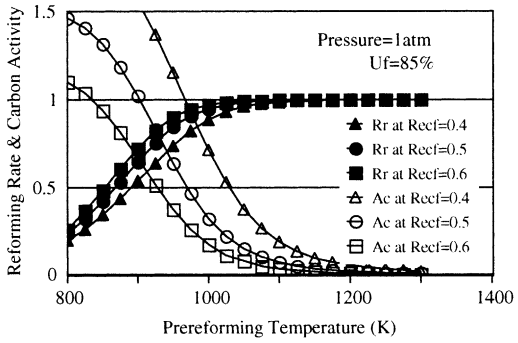

Fig. 2. Dependence of reforming rate, R_r, and carbon activity, A_c on reforming temperature and fuel recirculation at equilibrium.

The pre-reforming temperature of the developed SOFC was 973 K [8]. As can be seen in Fig. 2, at the fuel recirculation rate of 0.4, carbon formation may take place at 970 K. This temperature has no margin for the above-mentioned pre-reforming temperature. Therefore, the fuel recirculation rate is set at 0.5 at which the carbon formation temperature is 900 K.

The pre-reforming rate of CH_4 has to be smaller than the value given in Fig. 2 due to the slow reforming reaction and the limit of the pre-reformer size.

4.1.2. Internal reforming

After appropriate pre-reforming, the fuel containing residual methane goes into the internal reformer. The rate of the reforming reaction, R_{CH_4}, of Eq. (3) is given as [9]

$$R_{CH_4} = 1.75 \exp\left(\frac{-57840}{RT}\right) P^{1.2}_{CH_4}. \tag{9}$$

The change in the methane molar flow, dM_{CH_4}/dx, is given as

$$\frac{dM_{CH_4}}{dx} = -A_{ref} R_{CH_4} W_{cat}. \tag{10}$$

where A_{ref} is the reforming area per unit length of the internal reformer (or cell), and W_{cat} the catalyst weight density.

With the advance of the methane reforming as given by Eq. (10), H_2 and CO are generated consuming CH_4 and H_2O as given by Eq. (3). At the same time, the water gas shift reaction given by Eq. (4) reaches equilibrium rapidly. Therefore, CO, CO_2, H_2 and H_2O have to satisfy the following equilibrium equation:

$$K_s = \frac{X_{CO_2} X_{H_2}}{X_{CO} X_{H_2O}}, \tag{11}$$

where K_s is the equilibrium constant of Eq. (4). The atomic conservation of C, H and O has also to be kept

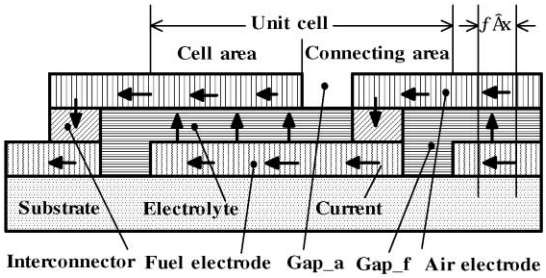

Fig. 3. Cross-sectional view of segmented type cell stack.

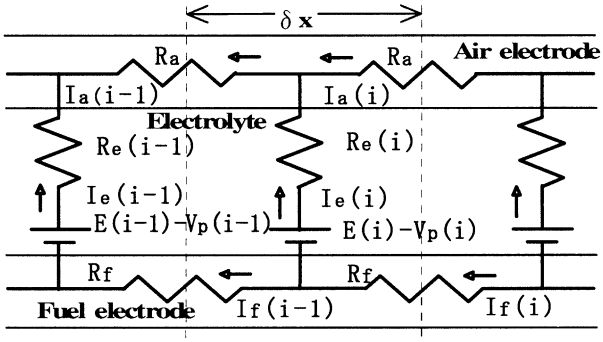

Fig. 4. Equivalent ladder circuit of cell area.

among CO_2, H_2 and H_2O, excluding CH_4, which is not in equilibrium.

4.2. Cell

4.2.1. Equivalent electrical circuit of cell

The segmented type tubular cell stack consists of many pairs of cells and interconnectors. Fig. 3 shows a part of the cross-section of the stack. The corresponding equivalent ladder circuit of the cell area is shown in Fig. 4.

In the connecting area, a similar circuit without the local electromotive force can be drawn to calculate the voltage drop. Each resistance and the related values of typical cell components at 1273 K are given in Table 1. These values were obtained from the literature [10].

The resistivity of the electrolyte strongly depends on the temperature, and its effect cannot be ignored. The dependence of resistivity on the temperature is given by the following equation [11]:

$$R_e = R_{e0} \exp\left[10100\left(\frac{1}{T} - \frac{1}{1273}\right)\right]. \tag{12}$$

The resistivities of other parts are assumed to be constant because these resistivities depend weakly on temperature [12], and their contributions to the total voltage drop are small.

Each branch current can be obtained by the iterative method, giving an electromotive force E and a polarization voltage V_p. The method of calculating the electromotive force and the polarization will be given in the following sections.

Finally, the cell voltage and then the output voltage of the stack can be obtained. This enables calculating the efficiency by Eq. (1).

4.2.2. Changes in gaseous component, electromotive force and concentration polarization in cell stack

The changes in molar fractions of the fuel in the cell stack have to be calculated considering the reforming of residual methane and the inflow of oxygen due to the cell reaction.

In this region, CO, CO_2, H_2 and H_2O have to satisfy the equilibrium equation given in Eq. (11). However, in atomic conservation, an increase in O due to the cell reaction has to be considered.

The ideal electromotive force of the relevant position, E, is given as

$$E = E_0(T) + \frac{RT}{2F} \ln \frac{X_{H_2}\sqrt{P'_{O_2}}}{X_{H_2O}}, \tag{13}$$

The concentration polarization is the difference between the ideal local electromotive force and the real electromotive force. The real local electromotive force can be given in the same manner as Eq. (13) using molar fractions at the interfaces between the electrode and the electrolyte. The concentration polarization of the relevant position, V_{cons}, is then given as

$$V_{cons} = \frac{RT}{2F} \ln \frac{X_{H_2} X_{H_2O,B} \sqrt{X'_{O_2}}}{X_{H_2,B} X_{H_2O} \sqrt{X'_{O_2,B}}}, \tag{14}$$

These molar fractions also have to satisfy Eq. (11). To obtain V_{cons}, the mass fluxes in the electrodes and the substrate have to be calculated.

In porous media, only radial flow is assumed at the active cell area, and no flow is assumed in the interconnecting area.

Table 1
Resistance and diffusion parameters at 1273 K [10][a]

Component	Thickness (cm)	Resistivity (Ω cm)	Resistance (Ω)
Air electrode (Sr doped $LaMnO_3$)	0.1	0.013	$R_a = 0.0184\delta x$
Electrolyte (Y_2O_3 doped ZrO_2: YSZ)	0.005	10.0	$R_{e0} = 0.00745/\delta x$
Fuel electrode (40 vol.% Ni/YSZ cermet)	0.015	0.001	$R_f = 0.01003\delta x$
Interconnector (Mg doped $LaCrO_3$)	0.003	0.5	$R_{int} = 0.00022/\delta x$

[a] Total stack length = 108 cm; unit cell length = 1.2 cm active area plus 0.6 cm connecting area; substrate: outer diameter D = 2.1 cm, thickness = 0.2 cm; porosity ε = 0.4 (common in electrodes and substrate).

Here, we define the current density J as the current density at the surface of the substrate

$$J = \frac{I_e}{2\pi r_{sub}\delta_x}. \quad (15)$$

The molar fluxes of the gas components in porous media have the following relations:

$$N_{H_2} + N_{CO} = \left(\frac{r_{sub}}{r}\right)\frac{J}{2F}, \quad (16a)$$

$$N_{H_2O} = -N_{H_2}, \quad N_{CO_2} = -N_{CO}, \quad (16b)$$

$$N_{O_2} = -\left(\frac{r_{sub}}{r}\right)\frac{J}{4F}, \quad N_{N_2} = 0. \quad (16c)$$

The effect of the direct oxidation of methane to contribute to Eq. (16) is neglected because its oxidation speed is slow. The gaseous flows in the porous media are assumed to be governed by the Stefan–Maxwell equations as [13]

$$\frac{dX_i}{dr} = \sum_j \frac{X_i N_j - X_j N_i}{cD_{ij}}, \quad (17)$$

D_{ij} is given as [14]

$$D_{ij} = D^0_{ij}\varepsilon^2, \quad (18)$$

where $D^0_{ij}$is the diffusivity between gas species i and j in free space that can be calculated by the Chapman–Enskog equation [15] and ε the porosity of electrode or substrate.

The total molar density, c, is assumed to be constant at any position. The molar fractions at the main flow and the interface can be calculated using Eqs. (9)–(11), (15)–(18). We can then calculate the concentration polarization by Eq. (14).

4.2.3. Activation polarizations

The activation polarization, V_{act}, was given by Sawata et al. as follows: [16]

$$J = J_0\left[\exp\left(\frac{2FV_{act}}{RT}\right) - \exp\left(\frac{-\alpha FV_{act}}{RT}\right)\right], \quad (19)$$

where

$$J_0 = \frac{\sigma_0 RT}{(2+\alpha)F}, \quad (20)$$

where α is the apparent transfer coefficient denoting unsymmetrical reaction, σ_0 the interface conductivity. Setoguti et al. [17] suggested that σ_0 for the fuel electrode mainly depends on the residual oxygen pressure in the fuel. However, that relation is complicated. Here we simplify the dependence of σ_0 on the oxygen pressure, $P_{O_2,B}$, as follows:

$$\sigma_0 = \beta\exp\left(\frac{-\Delta G_{act}}{RT}\right)P^{\gamma}_{O_2,B}, \quad (21)$$

where β is a constant, γ the reaction order, ΔG_{act} the activation energy. In the oxidant, $P_{O_2,B} = P'_{O_2,B}$. In the fuel, the oxygen pressure is given as

$$P_{O_2,B} = \left(\frac{P_{H_2O,B}}{K_{ox}P_{H_2,B}}\right)^2, \quad (22)$$

Yamamoto et al. [18] suggested that γ for the air electrode was approximately 0.5.

From our small experiments and these references, each coefficient is given as shown in Table 2.

Table 2
Coefficients to give activation polarization

Position	α	β	γ	ΔG_{act} (kJ/mol)
Fuel electrode	1	$10^{7.79}$	0.133	120
Air electrode	2	$10^{6.02}$	0.5	130

The activation polarization $V_{act,ox}$ in the oxidant and the activation polarization $V_{act,f}$ in the fuel can be calculated numerically using Eqs. (19)–(22). The total polarization is then given as

$$V_p = V_{cons} + V_{act,ox} + V_{act,f}. \quad (23)$$

4.2.4. Total voltage drop and cell voltage

Now we can calculate the current distribution and then the voltage drop in the cell stack. The average voltage drop and the average cell voltage are shown in Fig. 5. The simulated cell voltage of this figure agrees well with that reported by Singhal [19] as seen in Fig. 5.

4.3. Enthalpy balance

The enthalpy balance is calculated using the control-volume method [20]. The term control-volume is abbreviated as CV here. The dimension of the specified control-volume along flow direction is taken as δx.

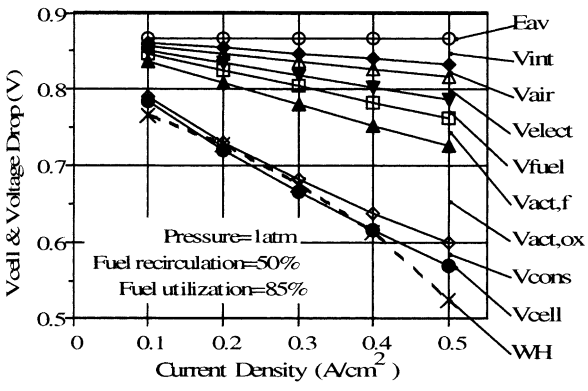

Fig. 5. Average voltage drop and cell voltage vs. current density at 1273 K. E_{av}: average electromotive force; V_{cell}: average cell voltage; V_{ine}: average ohmic voltage drop in interconnector; V_{fuel}: average ohmic voltage drop in fuel electrode; V_{air}: average ohmic voltage drop in air electrode; V_{elect}: average ohmic voltage drop in electrolyte; WH: V_{cell} reported by Singhal of SWHPC.

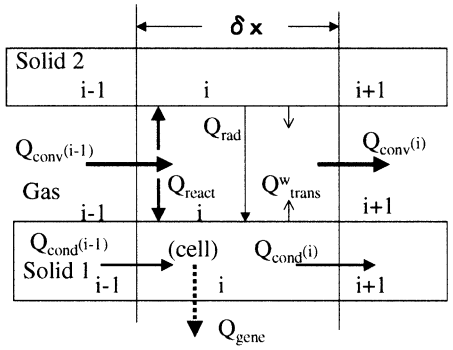

Fig. 6. Enthalpy balance in CVs of solid and gas phases.

All solids are assumed to be uniform solids having the equivalent thermal conductivities of multilayers.

All the chemical reactions are assumed to take place in the solids (catalyst, electrodes, interfaces of electrode and electrolyte). The schematic heat migration in the solid CV and the gas CV is shown in Fig. 6. Each CV is numbered sequentially as CV($i-1$), CV(i), CV($i+1$). Here, the heat migration from CV($i-1$) to CV(i) due to heat conduction is denoted as $Q_{\mathrm{cond}}(i-1)$, the heat migration due to the convection is denoted as $Q_{\mathrm{conv}}(i-1)$, and so on.

4.3.1. Enthalpy balance in gas CV

The increase in the enthalpy in CV lying between x and $x+\delta x$ has to balance the enthalpy input from the side walls. For the gas CV(i) (see Fig. 6),

$$Q_{\mathrm{conv}}(i) - Q_{\mathrm{conv}}(i-1) = Q^{\mathrm{g}}_{\mathrm{cond}} + \sum Q^{\mathrm{w}}_{\mathrm{trans}} - Q_{\mathrm{react}}, \tag{24}$$

where

$$Q_{\mathrm{conv}}(i) = \sum_j M_j H_j(T_{\mathrm{g}}(i)), \tag{25}$$

$$H_j(T_{\mathrm{g}}(i)) = H^0_j(T_0) + \int_{T_0}^{T\mathrm{g}(i)} C_{pj}\,\mathrm{d}T. \tag{26}$$

Each enthalpy on the right side of Eq. (24) is given as follows:

$$Q^{\mathrm{g}}_{\mathrm{cond}} = [T_{\mathrm{g}}(i+1) + T_{\mathrm{g}}(i-1) - 2T_{\mathrm{g}}(i)]\frac{k_{\mathrm{g}}A_{\mathrm{g}}}{\delta x}, \tag{27}$$

$$Q^{\mathrm{w}}_{\mathrm{trans}} = S_{\mathrm{s}}h_{\mathrm{g}}[T_{\mathrm{s}}(i) - T_{\mathrm{g}}(i)], \tag{28}$$

$$Q_{\mathrm{react}} = Q_{\mathrm{reform}} + Q_{\mathrm{shift}}, \quad (\text{for the fuel in the internal reforming region}) \tag{29a}$$

$$Q_{\mathrm{react}} = Q_{\mathrm{cell,ox}}, \quad (\text{for the oxidant in the cell region}) \tag{29b}$$

$$Q_{\mathrm{react}} = Q_{\mathrm{reform}} + Q_{\mathrm{shift}} + Q_{\mathrm{cell,f}}, \quad (\text{for the fuel in the cell region}) \tag{29c}$$

$$Q_{\mathrm{react}} = 0, \quad (\text{for other region}) \tag{29d}$$

where

$$Q_{\mathrm{reform}} = \delta M_{\mathrm{CH_4}}[H_{\mathrm{CH_4}}(T_{\mathrm{g}}(i)) + H_{\mathrm{H_2O}}(T_{\mathrm{g}}(i)) - 3H_{\mathrm{H_2}}(T_{\mathrm{s}}(i)) - H_{\mathrm{CO}}(T_{\mathrm{s}}(i))], \tag{30}$$

where $\delta M_{\mathrm{CH_4}}$ moles of reformed CH_4 in solid CV(i) that can be calculated using Eq. (10),

$$Q_{\mathrm{shift}} = \delta M_{\mathrm{CO_2}}[H_{\mathrm{CO}}(T_{\mathrm{g}}(i)) + H_{\mathrm{H_2O}}(T_{\mathrm{g}}(i)) - H_{\mathrm{H_2}}(T_{\mathrm{s}}(i)) - H_{\mathrm{CO_2}}(T_{\mathrm{s}}(i))], \tag{31}$$

where $\delta M_{\mathrm{CO_2}}$ is the moles of CO_2 generated by the water gas shift reaction in solid CV(i) that can be calculated using Eq. (11) and atomic conservation. If $\delta M_{\mathrm{CO_2}}$ is negative, $T_{\mathrm{g}}(i)$ and $T_{\mathrm{s}}(i)$ in the second term on the right-hand side of Eq. (31) have to be exchanged:

$$Q_{\mathrm{cell,ox}} = \frac{I_{\mathrm{e}}(i)}{4F}H_{\mathrm{O_2}}(T_{\mathrm{ox}}(i)), \tag{32}$$

$$Q_{\mathrm{cell,f}} = \delta M_{\mathrm{H_2}}[H_{\mathrm{H_2}}(T_{\mathrm{f}}(i)) - H_{\mathrm{H_2O}}(T_{\mathrm{cell}}(i))] + \delta M_{\mathrm{CO}}[H_{\mathrm{CO}}(T_{\mathrm{f}}(i)) - H_{\mathrm{CO_2}}(T_{\mathrm{cell,f}}(i))], \tag{33}$$

where $\delta M_{\mathrm{H_2}}$ and δM_{CO} can be obtained using $N_{\mathrm{H_2}}$ and N_{CO} as solutions for Eqs. (16) and (17).

4.3.2. Enthalpy balance in solid CV

The enthalpy balance in CV of solid is given as

$$Q_{\mathrm{cond}}(i) - Q_{\mathrm{cond}}(i-1) = \sum Q_{\mathrm{rad}} + Q_{\mathrm{react}} - \sum Q^{\mathrm{w}}_{\mathrm{trans}} - Q_{\mathrm{gene}}, \tag{34}$$

where

$$Q_{\mathrm{cond}}(i) = -A_{\mathrm{s}}k_{\mathrm{s}}\frac{T_{\mathrm{s}}(i+1) - T_{\mathrm{s}}(i)}{\delta x}, \tag{35}$$

and Q_{rad} is the enthalpy input due to radiation from neighboring solid CVs [21], Q_{react} and $Q^{\mathrm{w}}_{\mathrm{trans}}$ the same as those defined in the preceding section and Q_{gene} the cooling due to power generation for the cell.

Each enthalpy on the right-hand side of Eq. (34) is given as follows:

$$Q_{\mathrm{rad}} = \frac{5.67(T^4_{\mathrm{sx}} - T^4_{\mathrm{s}}(i))10^{-12}}{1/(\varepsilon_{\mathrm{s}}S_{\mathrm{s1}}) + (1/(\varepsilon_{\mathrm{s}} - 1))/S_{\mathrm{s2}}}, \tag{36}$$

$$Q_{\mathrm{react}} = Q_{\mathrm{reform}} + Q_{\mathrm{shift}}, \quad (\text{for the internal reformer}) \tag{37a}$$

$$Q_{\mathrm{react}} = Q_{\mathrm{reform}} + Q_{\mathrm{shift}} + Q_{\mathrm{cell,f}} + Q_{\mathrm{cell,ox}}, \quad (\text{for the cell}) \tag{37b}$$

$$Q_{\mathrm{react}} = 0, \quad (\text{for the solid parts}) \tag{37c}$$

$$Q_{\mathrm{gene}} = 0, \quad (\text{except for the cell part}) \tag{38a}$$

$$Q_{\mathrm{gene}} = I_{\mathrm{e}}(i)[E(i) - V_{\mathrm{p}}(i) - I_{\mathrm{e}}(i)R_{\mathrm{e}}(i)] - \frac{[I^2_{\mathrm{a}}(i)R_{\mathrm{a}} + I^2_{\mathrm{a}}(i-1)R_{\mathrm{a}} + I^2_{\mathrm{f}}(i)R_{\mathrm{f}} + I^2_{\mathrm{f}}(i-1)R_{\mathrm{f}}]}{2}. \quad (\text{for the cell}) \tag{38b}$$

Table 3
Thermal conductivities at 1273 K [25,26]

Component	Thermal conductivity (W/(cm K))	Component	Thermal conductivity (W/(cm K))
Air electrode	0.02	Interconnector	0.02
Electrolyte	0.027	Internal reformer, air tube (Al_2O_3)	0.03
Fuel electrode	0.11	Substrate (CSZ)	0.01

In the connecting area, $V_p(i)$ vanishes in Eq. (38a), and the currents and resistances have to be replaced by appropriate values matching the position.

Since the Reynolds numbers of die fuel and the oxidant are under 500, die heat transfer coefficient, h_g, is calculated using a fully developed laminar flow approximation at constant wall temperature as [22]

$$h_g = \frac{3.66\,k_g}{d_e} \tag{39}$$

where k_g is the thermal conductivity of the mixed gas, d_e the equivalent diameter, k_g the calculated using the Bromley–Wike equation [23]. The thermal conductivities of gases are taken from the data book [24]. The thermal conductivities of the solid components are given in Table 3. The dependence of these values on temperature is ignored for simplicity.

The calculated typical temperature distributions are shown in Fig. 7. The temperature distribution of the cell stack is moderate, and the average temperature is 1260 K. There is no literature to refer to concerning this temperature distribution. However, the tendency of the temperature distribution of the cell stack agrees well with that of 3 kW SOFC of WH [27].

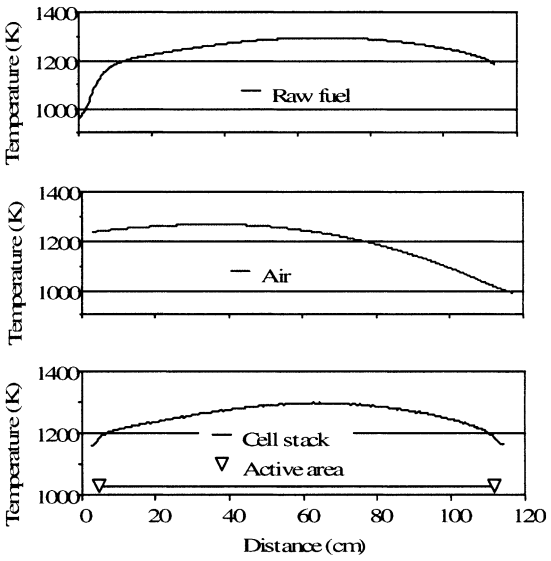

Fig. 7. Example of temperature distributions in a cell stack. T_{fin}: 953 K; T_{ain}: 993 K; U_f: 85%; U_{ox}: 50%; fuel and oxidant recirculation: 50%; internal reforming: 90%; catalyst density: 2.3 mg/cm^2.

4.3.3. Exhaust temperature

The exhaust temperature can be obtained from the following global heat balance:

$$\sum_j^{\text{exhaust}} M_j H_j(T_{out}) = \sum_j^{\text{input air}} M'_j H_j(T_{a0}) + M_{CH_4} H_{CH_4}(T_{f0}) - V_t I_0 \tag{40}$$

For the input air,

$$M'_{O_2} = 2M_{CH_4}\frac{U_f}{U_{ox}}, \qquad M'_{N_2} = \left(\frac{0.79}{0.21}\right)M'_{O_2}, \tag{41}$$

where Ar, CO_2 and other elements are neglected as components of air.

For the exhaust gas,

$$M_{O_2} = 2M_{CH_4}\left(\frac{U_f}{U_{ox}}\right) - 1, \qquad M_{N_2} = M'_{N_2} \tag{42}$$

$$M_{CO_2} = M_{CH_4}, \qquad M_{H_2O} = 2M_{CH_4}. \tag{43}$$

5. Procedure for numerical results

The main results desired are the current distribution, the gas component distribution and the temperature distribution. Each computation is carried out using die corresponding models. An algorithm to obtain numerical results is given in Fig. 8. Each computation step is executed using the results given in the former computation steps. The cycle of the computation steps is repeated until global convergence is obtained.

The effect of CV size on the computation results is given in Table 4. However, the size has little effect on the results. Therefore, the CV size is taken at 0.3 cm for the speed of convergence of the computation.

6. Specification of operating conditions of SOFC system

The fuel utilization, U_f, is set at 85% referring to the reported experiments as mentioned in Section 3.

The target value of the efficiency of an SOFC operating at 1273 K is about 50% (HHV) [28]. Therefore, V_{cell} has to be about 0.68 V as deduced from Eq. (1). As seen in Fig. 5, the cell voltage of 0.68 V can be obtained at a current density of about 0.3 A/cm^2; therefore, the current density is set at 0.3 A/cm^2.

The inlet temperature of the raw fuel, T_{f0} (see Fig. 1), is preset at 288 K. The inlet temperature of the air, T_{a0} (see Fig. 1), is the same. This temperature, 288 K, is the representative ambient temperature adopted in gas turbine systems [29].

The pre-reforming temperature (equal to preheated temperature of the fuel), T_{fin} (see Fig. 1), is set at 953 K. This

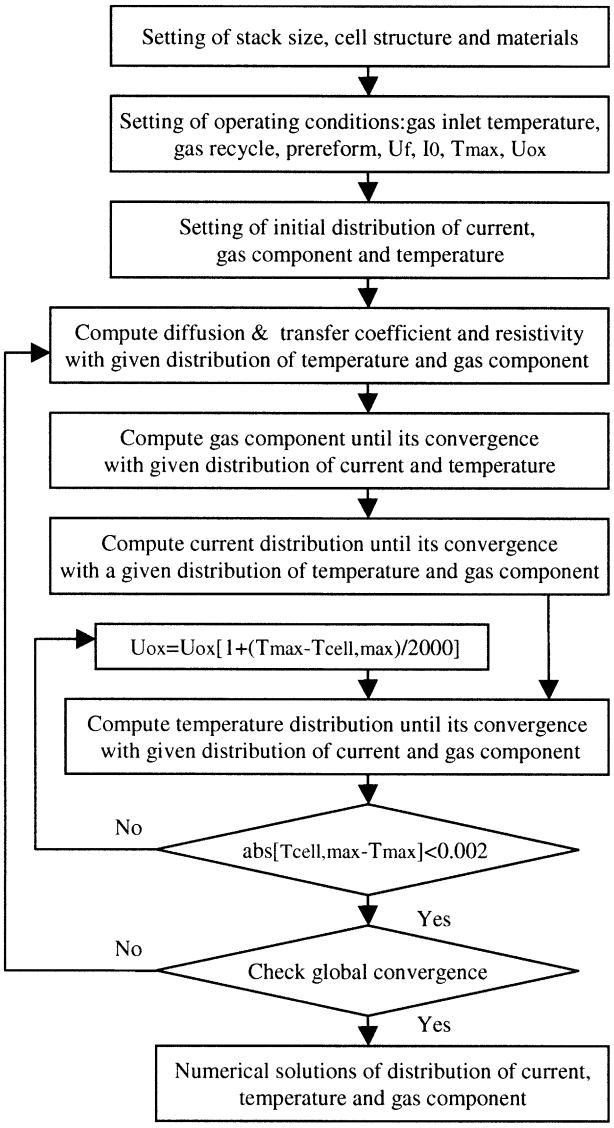

Fig. 8. Algorithm to obtain numerical results.

temperature is the value which is approximate to the reported reforming temperature [8] and avoids the formation of carbon. The preheated air temperature, (see Fig. 1), is set at 993 K. By setting these preheated temperatures, the temperature difference between the maximum temperature and minimum temperature can be limited to within 113 K as seen in Fig. 7.

The operating pressure of the cell stack is set at 1.0 atm. Though it is necessary to carry out a slight pressurization, this effect is neglected for simplicity.

Table 4
Effect of CV size on results

δx (cm)	η_{dc} (%)	U_{ox} (%)	T_{out} (K)
0.3	48.397	49.961	959.45
0.15	48.455	49.938	958.55

The fuel recirculation rate is set at 50% to suppress carbon formation as described in Section 4.1.1. The oxidant recirculation rate is also set at 50%, but there is no reason to set this value. However, the effect of recirculation will be discussed later.

The internal reforming rate is set at 90% (equal to 10% pre-reforming) in order to increase the cooling effect by the internal reforming. For this reforming rate, the catalyst density is set to 2.3 mg/cm^2 by trial and error. The pre-reforming of 10% is a value considering the progress of some reforming in the mixing of raw fuel and recycled fuel.

These operating conditions are chosen to obtain a moderate temperature distribution in the cell stack. The effects of these operation conditions of an SOFC system will be discussed later.

The maximum temperature of the cell stack is set at 1300 K by adjusting the oxygen utilization rate.

With this maximum temperature and these system operating conditions, we can obtain the average cell temperature of 1260 K which is almost equal to the 1273 K for the state-of-the-art of the operation temperature of the SOFC [27].

7. Results of simulation and discussion

7.1. Effect of catalyst density

By setting the appropriate uniform catalyst density in the internal reformer, the reforming rate reaches approximately 95% at the outlet of the internal reformer, as shown by curve (B) in Fig. 9. In the case, the temperature distribution of the cell is moderate, as shown by curve (b) in Fig. 10.

In the case of a thin catalyst density, the reforming rate at the outlet of the internal reformer is not sufficient as shown

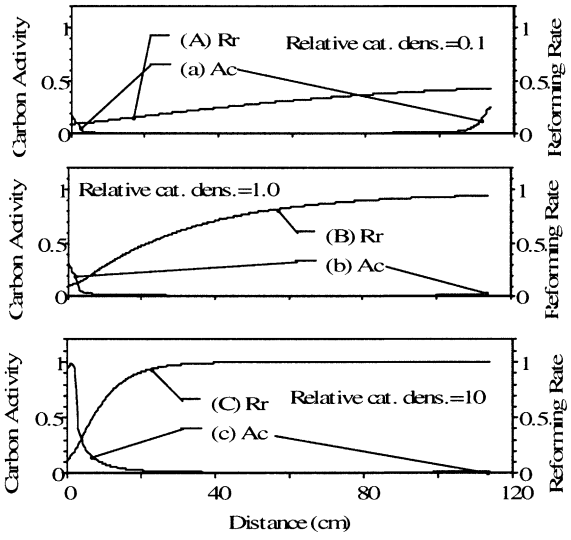

Fig. 9. Effect of catalyst density in internal reformer on reforming rate, R_r, and activity of carbon, A_c. The relative catalyst density 1.0 corresponds to 2.3 mg/cm^2.

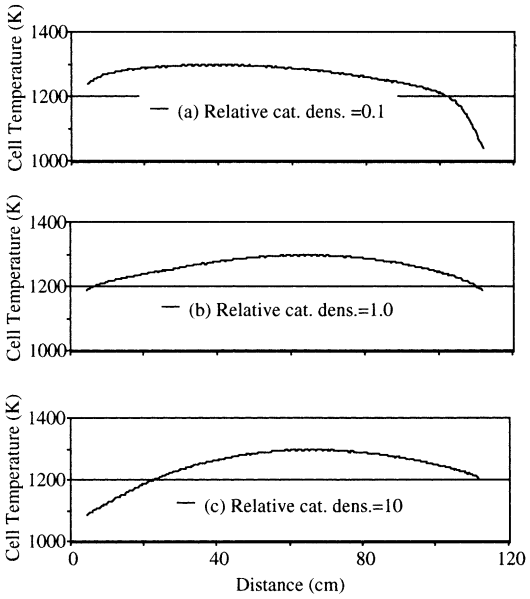

Fig. 10. Effect of catalyst density on cell temperature.

by curve (A) in Fig. 9. Therefore, much methane not yet reformed remains. This methane is reformed quickly at the fuel inlet region (at the right end of the cell) decreasing the cell temperature as shown by curve (a) in Fig. 10, because the fuel electrode acts as a thick catalyst for reforming.

On the contrary, in the case of a thick catalyst density, the reforming occurs quickly at the inlet region of the internal reformer, decreasing the neighboring cell temperature as shown by curve (c) in Fig. 10. This decrease in the temperature increases the carbon activity, A_c, to nearly 1.0 as shown by curve (c) in Fig. 9.

The catalyst density also affects the efficiency, the oxygen utilization and the exhaust temperature. The maximum exhaust temperature, T_{out}, and oxygen utilization, U_{ox}, can be obtained at a moderate catalyst density as shown in Fig. 11. However, the effect on the efficiency is insignificant.

7.2. Effect of internal reforming

In this section, the effect of the internal reforming rate is discussed with the relative catalyst density one given in the

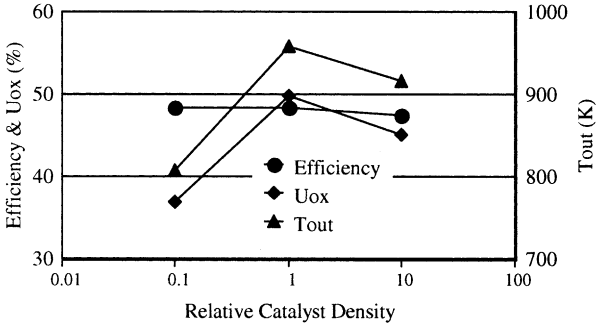

Fig. 11. Effect of catalyst on output characteristics.

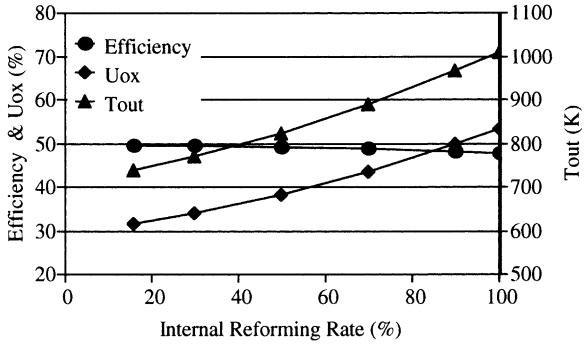

Fig. 12. Effect of internal reforming.

preceding section. As mentioned above, the reforming is a strongly endothermic reaction. Therefore, the increase in the internal reforming rate needs a decrease in the air flow rate (namely, an increase in the oxygen utilization U_{ox}) to keep the total cooling capacity at the same level. As a result, the increase in the internal reforming rate decreases the electromotive force and hence decreases the efficiency, as shown in Fig. 12. The decrease in the air flow increases the exhaust temperature.

7.3. Effect of graded catalyst distribution

In the previous sections, the catalyst density was uniform throughout the internal reformer. In this section, the effect of the graded catalyst density will be discussed. The rate of internal reforming is kept constant at 90%.

The total area of the internal reformer is divided into several regions of equal length. The setting of the catalyst density for each region is so calculated as to obtain the maximum efficiency, while the total catalyst weight is kept constant and the gradient of the density distribution is the upper right ascent. The obtained catalyst density for each region depends on the number of divisions as shown in Fig. 13.

The effect of the number of the regions on the cell temperature distribution is shown in Fig. 14. The curve for one region is omitted because it is the same as

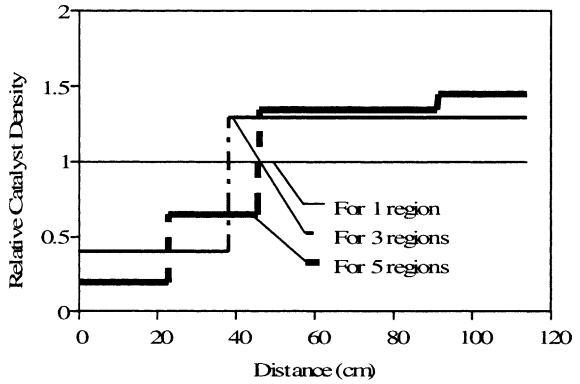

Fig. 13. Distribution of graded catalyst density. Internal reforming, 90%.

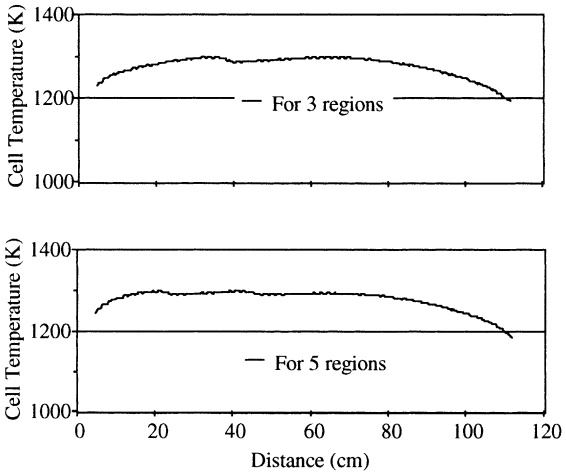

Fig. 14. Effect of number of regions of graded catalyst density on cell temperature distribution.

Fig. 10(b). As shown in the figure, the increase in the average temperature of the cell stack with the increasing number of regions can be seen. This increase in the average temperature decreases the internal losses and therefore decreases the air flow rate for cooling the cell. However, this decrease in the air flow rate decreases the electromotive force. As a result, the efficiency and the exhaust temperature slightly increase as shown in Fig. 15.

7.4. Effect of air inlet temperature and oxidant recirculation

Here, the effect of each operating condition specified in Section 6 on the output characteristics will be examined. As mentioned in Section 2, part of exhaust oxidant is recirculated to heat the inlet air to T_{ain}. The effect of the air inlet temperature, T_{ain}, is shown in Fig. 16.

The air (oxidant) functions as a coolant. Therefore, the increase in the air inlet temperature needs an increase in the air flow rate (namely, a decrease in the oxygen utilization U_{ox}) to keep the cooling capacity at the same level. The increased air flow dilutes the combustion exhaust gas to decrease the exhaust temperature. On the other hand, the

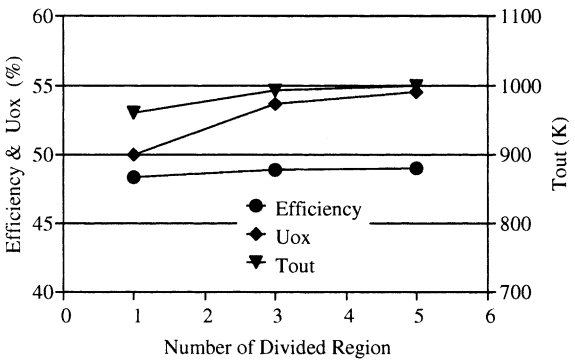

Fig. 15. Effect of number of regions of nonuniform catalyst densities.

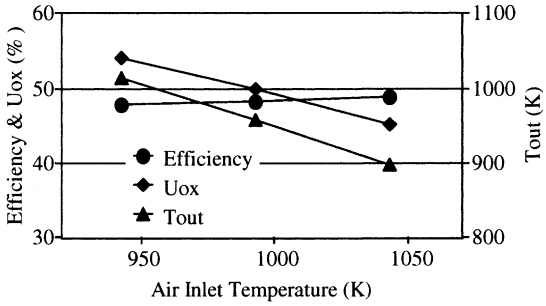

Fig. 16. Effect of air inlet temperature.

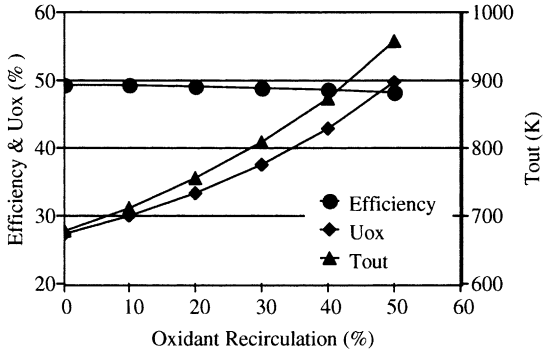

Fig. 17. Effect of oxidant recirculation.

increase in the air flow rate increases the output voltage and hence increases the efficiency. However, this effect is insignificant.

The effect of the oxidant recirculation is shown in Fig. 17. Here, T_{ain}, is kept constant at 993 K. The increase in the oxidant recirculation rate needs an increase in the oxidant utilization to keep the cooling capacity at the same level. The increase in the oxidant recirculation leads to a decrease in the oxygen partial pressure in the cell stack. Therefore, the increase in the oxidant recirculation decreases the cell.

7.5. Effect of raw fuel inlet temperature and fuel recirculation

The effect of the inlet temperature, T_{fin}, of the partially pre-reformed fuel is shown in Fig. 18. The increase in the

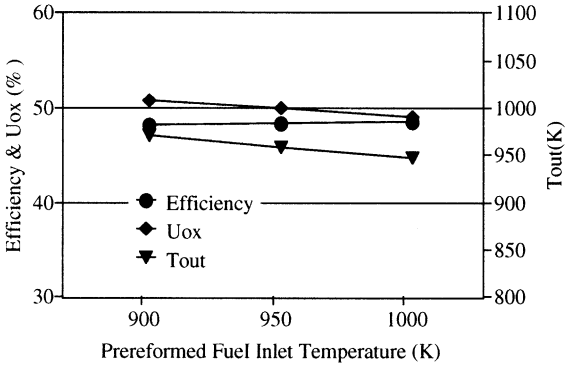

Fig. 18. Effect of pre-reformed fuel inlet temperature.

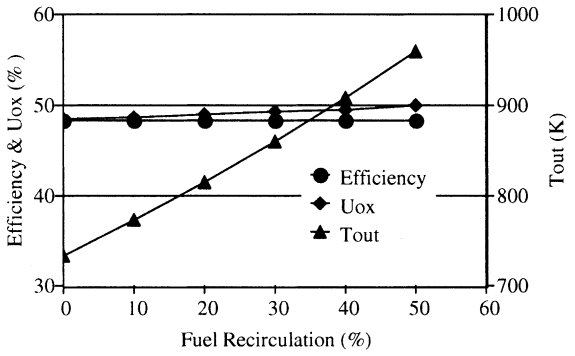

Fig. 19. Effect of fuel recirculation.

inlet temperature decreases the cooling capacity. Therefore, the flow rate of the air increases to compensate for the cooling capacity. The effect of the increase in the fuel inlet temperature resembles that of the increasing air inlet temperature. However, it is less effective because the heat capacity of the fuel is smaller.

The effect of the fuel recirculation is shown in Fig. 19. In this case, T_{fin} is kept constant at 953 K. To avoid carbon formation, water is added at the lower fuel recirculation. Therefore, the total cooling capacity of the fuel and the recirculated fuel is kept almost constant. Hence, the oxidant utilization only changes slightly. The efficiency hardly changes with the fuel recirculation rate, because the oxidant flow rate and the H_2/H_2O ratio in the fuel are kept at almost constant (namely, the electromotive force hardly changes). The heat necessary for the vaporization of the added water is supplied from the combustion exhaust gas in the pre-reformer. Therefore, the exhaust temperature from the SOFC system decreases with the decrease in the fuel recirculation.

8. Summary and conclusion

The effect of the internal reforming on the output characteristics of the SOFC system was discussed using numerical models. Some effects of gas inlet conditions have also been discussed. The following conclusions have been drawn for several sets of operating conditions of the SOFC system without the heat leak, restricting the maximum cell temperature at a constant 1300 K by adjusting the oxidant utilization rate.

1. Setting an appropriate uniform catalyst density leads to a moderate temperature distribution and leads to a higher temperature of the exhaust gas.
2. Increasing the internal reforming rate leads to a large increase in the exhaust temperature and leads to a slight decrease in the efficiency.
3. Setting the graded catalyst density leads to a flatter temperature distribution in the cell stack and leads to a slight increase in the exhaust temperature.
4. Increasing the inlet gas temperature, leads to a slight increase in the efficiency; however, leads to a decrease in the exhaust gas temperature from the SOFC system. The effect of the air inlet temperature on the exhaust temperature is significantly stronger than that of the fuel inlet temperature.
5. Increasing the oxidant recirculation leads to a slight decrease in the efficiency but leads to a large increase in the exhaust gas temperature. As for the fuel recirculation, the tendency is similar.

These results can be summarized as the operating conditions of the present SOFC system which have considerable effects on the exhaust temperature but a slight effect on the efficiency.

The effects of the heat leak and the pressurization will be investigated in the future in the relation with the combined power generation cycle.

References

[1] B.C.H. Steel, in: Proceedings of the International Symposium on SOFCs, Nagoya, 1989, p. 142.
[2] S.C. Singhal, Proc. Solid Oxide Fuel Cell 4 (1995) 205–207.
[3] H. Yokoyama, et al., Proc. Solid Oxide Fuel Cell 5 (1997) 99.
[4] S.C. Singhal, Proc. Solid Oxide Fuel Cell 6 (1999) 4145.
[5] J.R. Selman, in: L.J.M.J. Blomen, N.M. Mugerwa (Eds.), Fuel Cell Systems, Plenum Press, New York, 1993, pp. 360–361.
[6] P. Pietrogrande, M. Bezzeccheri, in: L.J.M.J. Blomen, M.N. Mugerwa, (Eds.), Fuel Cell Systems, Plenum Press, New York, 1993, p. 142.
[7] Hirshenbofer, et al. (Eds.), Fuel Cells: A Handbook, 1994, pp. 4–13.
[8] K. Sinozaki, et al., Fuel Cell Seminar Abstract, 1992, p. 359.
[9] R. Ødegard, et al., Proc. Solid Oxide Fuel Cell 4 (1995) 810–819.
[10] Hirshenhofer, et al. (Eds.), Fuel Cells: A Handbook, 1994, pp. 4–5.
[11] Y. Oono, et al., Trans. IEE Jpn. 106-b (8) (1986) 694 (Jpn.).
[12] D.W. Dees, et al., Fuel Cell Seminar Abstract, 1986, p. 58.
[13] R.B. Bird, et al., Transport Phenomena, Wiley, New York, 1960, p. 570.
[14] N. Wakao, J.M. Smith, Chem. Eng. Soc. 17 (1962) 832.
[15] R.B. Bird, et al., Transport Phenomena, Wiley, New York, 1960, p. 511.
[16] A. Sawata, et al., Solid State Ionics 40/41 (1990) 415–420.
[17] T. Setoguchi, et al., J. Electrochem. Soc. 139 (10) (1992) 2875–2880.
[18] O. Yamamoto, et al., J. Chem. Soc. Jpn. 8 (1988) 1324–1328 (Jpn.).
[19] S.C. Singhal, in: Proceedings of SOFC-VI, Yokohama, February 1995, p. 41.
[20] S.V. Patanker, Numerical Heat Transfer and Fluid Flow, Hemisphere Publishing Co., New York, 1980.
[21] Mark's Standard Handbook for Mechanical Engineers, 10th Edition, McGraw-Hill, New York, 1996, pp. 4-62–4-67.
[22] Heat Transfer Handbook, 4th Edition, JSME, 1986, 51 (Jpn.).
[23] L.A. Bromley, C.R. Wilke, Ind. Eng. Chem. 43 (7) (1951) 1645.
[24] Thermophysical Properties of Fluids, JSME, 1983, (Jpn.).
[25] Y. Kasuga, et al., Bull. Electrotech. Lab. 61 (7) (1997) 27–34 (Jpn.).
[26] K. Nakarnura, Z. Takehara, Bull. Chem. Soc. Jpn. 66 (10) (1993) 2800.
[27] A. Hirano, et al., J. Electrochem. Soc. 139 (10) (1992) 2748.
[28] K.A. Murugesamoortbi, et al., Fuel Cell Systems, in: J.M.J. Blomen, M.N. Mugerwa (Eds.), Plenum Press, New York, 1993, p. 465.
[29] Mark's Standard Handbook for Mechanical Engineers, 10th Edition, McGraw-Hill, New York, 1996, pp. 9–130.